6.1 Homogeneous Slope on Rigid Foundation

REFERENCE	Griffiths et al[1]
ELEMENTS	Plane strain elements
MODEL FILENAME	SlopeStability01.gts

Figure 6.1.1 shows the slope model with 21.57^{o} inclination subjected to self-weight. The left side of the model is constrained in the horizontal direction and the bottom side is completely fixed. Slope stability analysis is carried out using strength reduction method (SRM) during which the strength reduction factor (SRF) is gradually increased until instability is reached. The resulting factor of safety is compared with the reference solution.

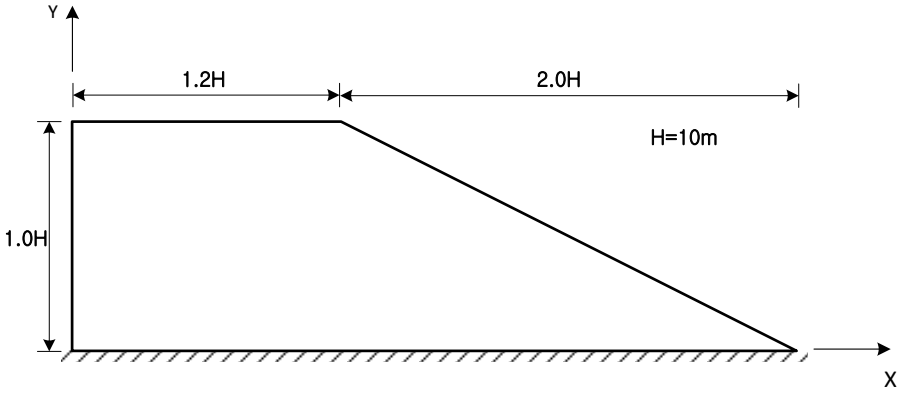

Figure 6.1.1
Slope model without foundation

Material data	Young's modulus	*E = 2.0 MPa*
	Poisson's ratio	$\nu = 0.3$
	Model type	*Mohr Coulomb*
	Cohesion	*10.0 kPa*
	Friction angle	*20 °*
	Dilatancy angle	*20 °*
Load data	Self weight	γ_t *=20.0 kN/m*^{3}

Figure 1.2.2
Normalized excess pore pressure distribution compared with analytical solution

Figure 6.1.2
Safety reduction factor vs. dimensionless displacement

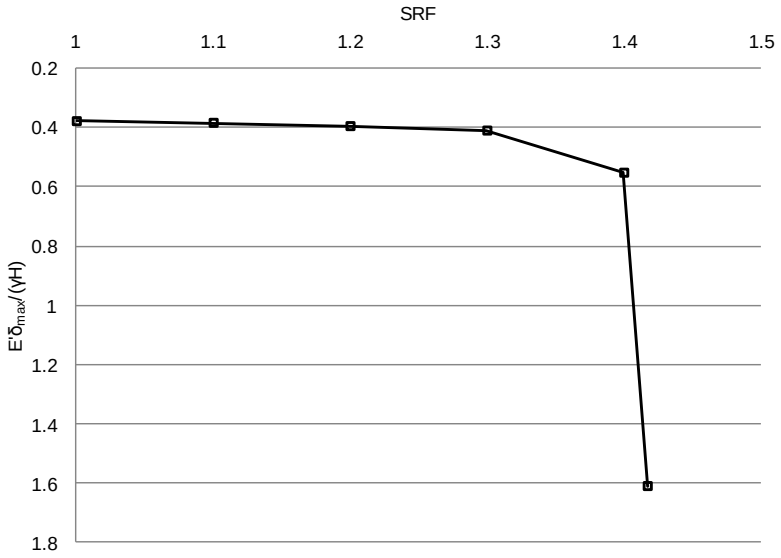

Table 6.1.1 Factor of safety at embankment

	Factor of safety
Reference	*1.4*
Quad-8	*1.4187*

Figure 6.1.3
Deformed shape and displacement contour at failure

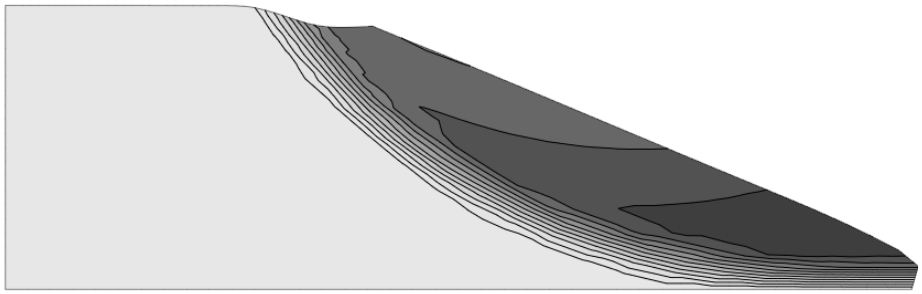

6.2 Two-sided Earth Embankment

REFERENCE	Griffiths et al[1]
ELEMENTS	Plane strain elements
MODEL FILENAME	SlopeStability02.gts

Figure 6.2.1 shows a dam model with phreatic surface which varies from the reservoir level to the foundation level. Slope stability analyses are carried out by strength reduction method (SRM) for two cases; A) with water level and B) without water level.

For both cases, the displacements are constrained in the horizontal direction along the vertical edges and in all directions along the bottom edge. The dam model is subjected to self weight and external pressure due to the existence of reservoir water (case A only). The resulting factors of safety are compared with the reference solutions.

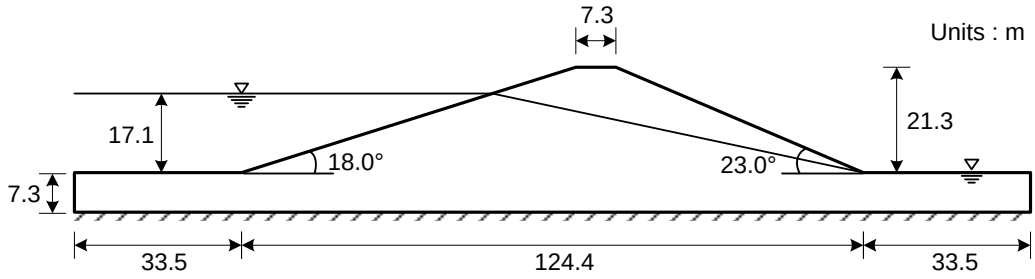

Figure 6.2.1
Two-sided earth embankment

Material data	Young's modulus	*E = 0.2 GPa*
	Poisson's ratio	$\nu = 0.3$
	Model type	*Mohr Coulomb*
	Cohesion	*13.8 kPa*
	Friction angle	*37 °*
	Dilatancy angle	*37 °*
Load data	Self weight	$\gamma_t = 18.2\ kN/m^3$

Table 6.2.1 Factor of safety at embankment

	Case A) with water level	Case B) without water level
Reference	*1.90*	*2.42*
Quad-8	*1.9656*	*2.5094*

Figure 6.2.2
Safety reduction factor vs. dimensionless displacement

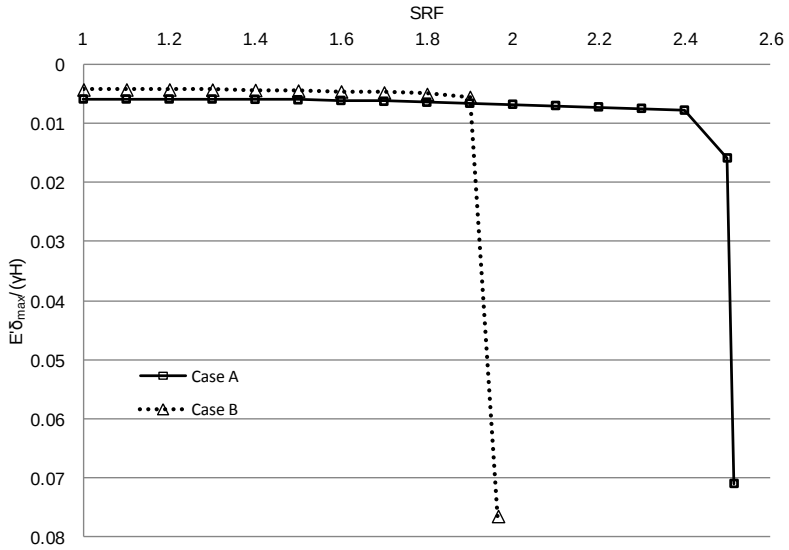

Figure 6.2.3 shows the deformed shape of the model in the vicinity of unstable equilibrium point for both with and without water level. For both cases, the instability occurs in the region where the slope is steeper. It is also noteworthy that if water is considered (case A), failure mechanism extends deeper into the foundation while, case B results in a toe failure. These results are in agreement with the limit equilibrium solutions included in the reference.

Figure 6.2.3
Deformed shape at failure

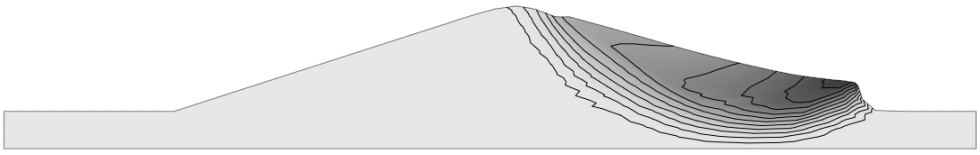

(case A)

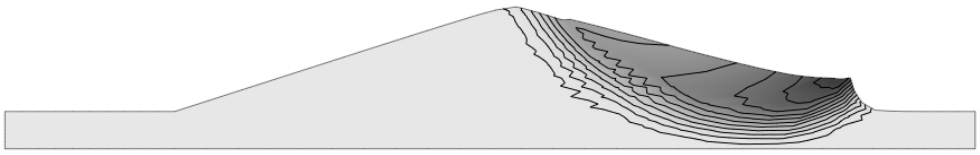

(case B)

6.3 Failure of Clay Slope with a Thin Weak Layer

REFERENCE	Griffiths et al[1]
ELEMENTS	Plane strain elements
MODEL FILENAME	SlopeStability03.gts

Figure 6.3.1 shows a slope on a foundation layer with embedded layer of weaker material to simulate a slippery liner within a landfill system. Slope stability analysis based on strength reduction method (SRM) is conducted. The displacements are constrained in the horizontal direction along the vertical edges and in all directions along the bottom edge. The slope system is subjected to self-weight.

While maintaining the strength of the soil, slope stability was evaluated for several strength values of the weak layer; C_{u2} / C_{u1} = 0.2, 0.4 and 1.0. Figure 6.3.2 shows the deformed shapes of the model in the vicinity of unstable equilibrium point for different strength values of the weak layer. The deformed shape matches the shape of the weak layer for C_{u2} / C_{u1} = 0.2 and turns to a circular shape as the model approaches homogeneous. Both failure mechanisms become active for C_{u2} / C_{u1} = 0.6.

These results illustrate the advantages of the finite element-based slope stability analysis which does not require a priori knowledge of the failure mechanism.

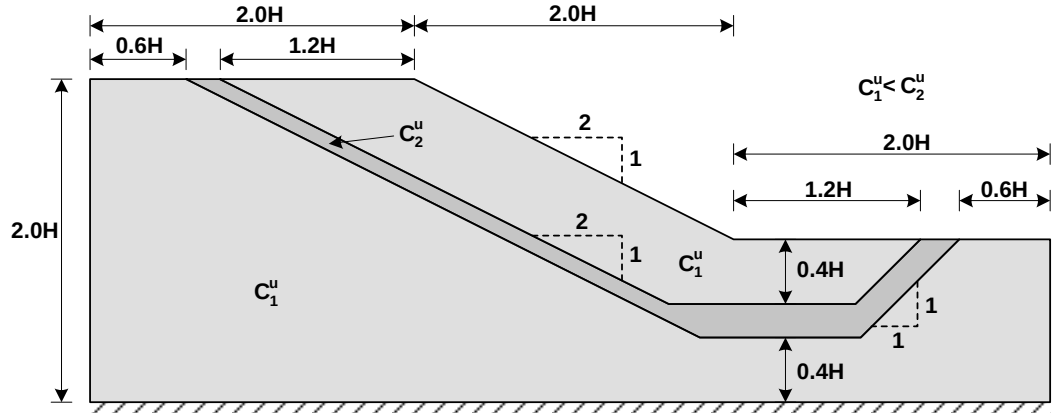

Figuree 6.3.1
Clay slope with a thin weak layer

Material data	Young's modulus	*E = 0.8 GPa*
	Poisson's ratio	*ν = 0.3*
	Model type	*Mohr Coulomb*
	Cohesion (C_{u1})	*50.0 kPa*
	Cohesion (C_{u2})	*20 kPa ~ 50.0 kPa*
	Friction angle	*0 °*
	Dilatancy angle	*0 °*
Load data	Self weight	*γ_t =20.0 kN/m^3*

Table 6.3.1 Factor of safety at embankment for C_{u2} / C_{u1} = 1.0

	Factor of safety
Reference	*1.47*
Quad-8	*1.4617*

Figure 6.3.2
Factor of safety for different values of C_{u2}/C_{u1}

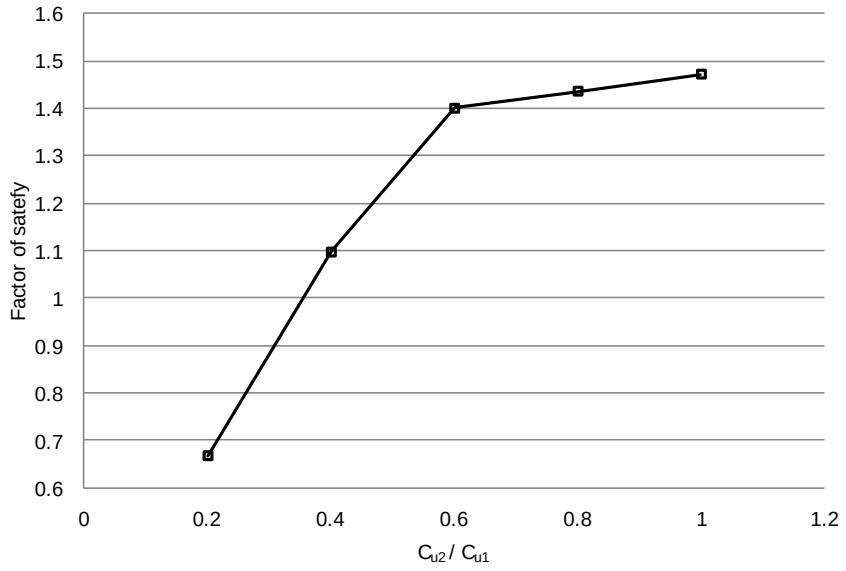

Figure 6.3.3
Deformed shape at failure for (a) C_{u2}/C_{u1} = 0.2, (b) C_{u2}/C_{u1} = 0.6, (c) C_{u2}/C_{u1} = 1.0

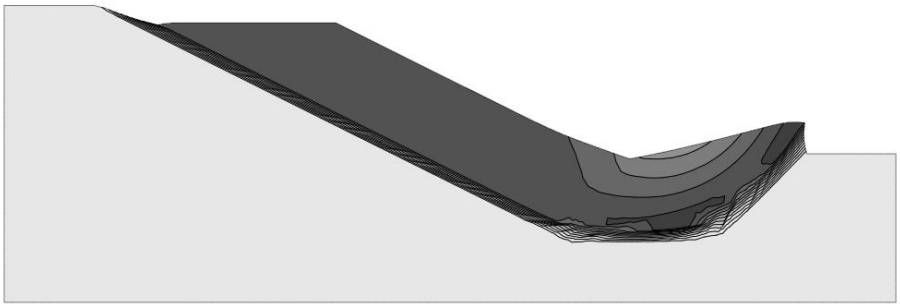

(a) C_{u2}/C_{u1} = 0.2

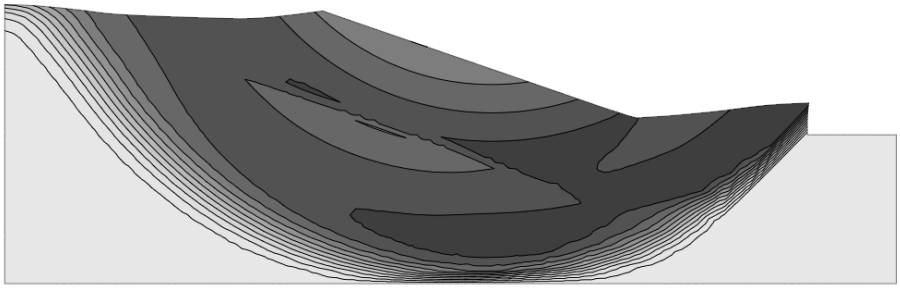

(b) C_{u2}/C_{u1} = 0.6

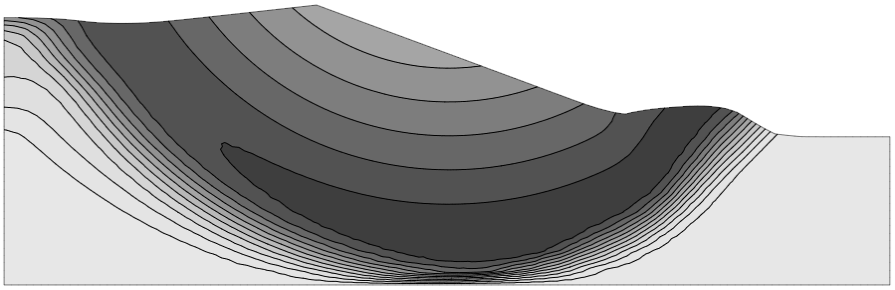

(c) C_{u2}/C_{u1} = 1.0

References

1 Griffiths, D.V. and Lane, P.A., "Slope stability analysis by finite elements", in Geotechnique, Vol. 49, No.3, pp.387-403, 1999